SLAC-PUB-11738
astro-ph/0602549

The relation between accretion rate and jet power in X-ray luminous elliptical galaxies

S.W. Allen[1], R.J.H. Dunn[2], A.C. Fabian[2], G.B. Taylor[3], C.S. Reynolds[4]
1. Kavli Institute for Particle Astrophysics and Cosmology, Stanford University, 382 Via Pueblo Mall, Stanford, CA 94305-4060, USA.
2. Institute of Astronomy, Madingley Road, Cambridge CB3 0HA, UK.
3. University of New Mexico, Department of Physics and Astronomy, Albuquerque, NM 87131, USA.
4. Department of Astronomy, University of Maryland, College Park, MD 20742, USA.

February 24, 2006

ABSTRACT
Using Chandra X-ray observations of nine nearby, X-ray luminous elliptical galaxies with good optical velocity dispersion measurements, we show that a tight correlation exists between the Bondi accretion rates calculated from the observed gas temperature and density profiles and estimated black hole masses, and the power emerging from these systems in relativistic jets. The jet powers, which are inferred from the energies and timescales required to inflate cavities observed in the surrounding X-ray emitting gas, can be related to the accretion rates using a power law model of the form $\log(P_{\rm Bondi}/10^{43}\,{\rm erg\,s^{-1}}) = A + B\log(P_{\rm jet}/10^{43}\,{\rm erg\,s^{-1}})$, with $A = 0.62 \pm 0.15$ and $B = 0.77 \pm 0.18$. Our results show that a significant fraction of the energy associated with the rest mass of material entering the Bondi accretion radius ($2.4^{+1.0}_{-0.7}$ per cent, for $P_{\rm jet} = 10^{43}\,{\rm erg\,s^{-1}}$) eventually emerges in the relativistic jets. Our results have significant implications for studies of accretion, jet formation and galaxy formation. The observed tight correlation suggests that the Bondi formulae provide a reasonable description of the accretion process in these systems, despite the likely presence of magnetic pressure and angular momentum in the accreting gas. The similarity of the $P_{\rm Bondi}$ and $P_{\rm jet}$ values argues that a significant fraction of the matter entering the accretion radius flows down to regions close to the black holes, where the jets are presumably formed. The tight correlation between $P_{\rm Bondi}$ and $P_{\rm jet}$ also suggests that the accretion flows are approximately stable over timescales of a few million years. Our results show that the black hole 'engines' at the hearts of large elliptical galaxies and groups feed back sufficient energy to stem cooling and star formation, leading naturally to the observed exponential cut off at the bright end of the galaxy luminosity function.

Key words: accretion, accretion disks – black hole physics – galaxies:active – galaxies:jets – X-rays: galaxies

1 INTRODUCTION

The black holes in the hearts of galaxies and galaxy clusters are commonly observed to be associated with powerful relativistic jets. The mechanism by which such jets form and the efficiency with which the energy associated with material entering the accretion radius is converted into jet power at much smaller radii remains the subject of much debate. Such knowledge is important for understanding the nature of the accretion process, galaxy formation and the growth of supermassive black holes.

X-ray studies with Chandra and XMM-Newton, building on earlier work with ROSAT, have shown that the black holes at the centres of galaxies, groups and clusters interact strongly with their environments, blowing clear cavities or 'bubbles' in the surrounding X-ray emitting gas (*e.g.* Böhringer *et al.* 1993; Fabian *et al.* 2000, 2003, 2005; Birzan *et al.* 2004; Forman *et al.* 2006). Simple arguments based on the energy required to inflate the bubbles and the sound speed of the surrounding gas allow these bubbles to be used as calorimeters, measuring the power released by the jets (*e.g.* Churazov *et al.* 2002). Importantly, the exquisite spatial resolution of Chandra means that for the largest, nearby ellipticals we are also able to resolve regions close to the Bondi accretion radii in these systems. Given estimates for the central black hole masses from measured galaxy velocity dispersions, the observed density and temperature profiles of the X-ray emitting gas can be used to estimate the accre-

Submitted to Mon.Not.Roy.Astron.Soc.

Work supported in part by Department of Energy contract DE-AC02-76SF00515

tion rates onto the black holes (Bondi 1952). Taken together, the accretion rates and jet powers then allow us to estimate the efficiency with which the rest mass of accreted matter is converted into jet power.

The observed luminosities of AGN in elliptical galaxies are typically several orders of magnitude lower than would be predicted from the standard Bondi formulae, assuming a conversion efficiency for matter into radiation of order 10 per cent. However, much of the predicted power may actually be released in the form of jets. This issue was investigated by Di Matteo *et al.* 2003 and Taylor *et al.* (2005) who noted that although the central AGN in M87, NGC4696 and NGC6166 have bolometric luminosities three orders of magnitude below the Bondi predictions (for 10 per cent efficiency), the jet powers inferred from the observed X-ray cavities are comparable, within a factor of a few. Here we extend this work to a sample of nine nearby, X-ray bright ellipticals with good X-ray data and optical velocity dispersion measurements.

The origin of the observed galaxy luminosity function and in particular the mechanism responsible for truncating star formation in the largest ellipticals is also a subject of much debate (*e.g.* Benson *et al.* 2003, Croton *et al.* 2005; Bower *et al.* 2005, and references therein). Here again, significant insight has been provided by XMM-Newton and Chandra observations (*e.g.* Tamura *et al.* 2001; Allen *et al.* 2001; Peterson *et al.* 2001, 2003) which show that the cooling rates in the cores of galaxies, groups and clusters are much smaller than the values predicted by simple models that do not include feedback. Some widespread form of heating must be operating in galaxies and clusters to stem cooling. We show that kinetic power released in jets from the central black hole engines can provide this power and stem further star formation.

2 OBSERVATIONS AND DATA ANALYSIS

2.1 Target selection

Our target galaxies are bright, nearby ellipticals with accurate central black hole mass measurements or velocity dispersions which allow the black hole masses to be estimated *e.g.* using the relation of Tremaine *et al.* (2004). The Chandra archive was searched to identify all such systems with X-ray luminous gaseous halos and obvious jet-induced cavities in the X-ray emitting gas. We have restricted our target list to those systems in which the bubbles are attached (or very close to) to the central AGN, which are therefore likely to be undergoing inflation. We have also required that the Chandra exposure times be sufficient to allow precise measurements of the central density and temperature of the X-ray emitting gas. Finally, we required that the X-ray data allow us to measure the properties of the X-ray emitting gas within one order of magnitude of the Bondi radius, permitting reliable measurements or extrapolations of the gas properties at that radius to be made. These selection criteria are matched by eight galaxies with data in the Chandra archive. For comparison purposes, we also include results for one more distant system, NGC6166, the dominant galaxy of Abell 2199. Although, due to its greater distance, we do not come close to resolving the Bondi radius in this system, the density profile follows a simple power-law form which allows an interesting extrapolation to smaller radii.

Table 1. Summary of the Chandra observations. Columns list the target name (and alternative), distance in Mpc, observation date and net exposure after all cleaning and screening procedures were carried out. For the Virgo Cluster ellipticals, a distance of 17 Mpc has been assumed. For NGC 507, 4696 and 5846 the distances are luminosity distances for a flat ΛCDM cosmology with $\Omega_{\rm m} = 0.3$ and a Hubble Constant $H_0 = 70\,{\rm km\,s^{-1}\ Mpc^{-1}}$.

	d_L (Mpc)	Date	Exposure (ks)
NGC507	71.4	2000 Oct 11	19.1
NGC4374 (M84)	17	2000 May 19	28.1
NGC4472	17	2001 Jun 12	21.9
NGC4486 (M87)	17	2000 Jul 29	33.7
NGC4552 (M89)	17	2001 Apr 22	53.4
NGC4636	17	2000 Jan 26	43.2
NGC4696	44.9	2004 Apr 01	86.7
NGC5846	24.6	2000 May 24	19.5
NGC6166	135.5	1999 Dec 11	15.0

2.2 Chandra analysis

The Chandra observations were carried out using the Advanced CCD Imaging Spectrometer (ACIS) between 1999 December and 2004 April. The ACIS-S array was used as the primary detector as it offers the best sensitivity to soft X-ray emission from the galaxies. The standard level-1 event lists produced by the Chandra pipeline processing were reprocessed using the *CIAO* (version 3.2.1) software package, including the latest gain maps and calibration products. Bad pixels were removed and standard grade selections applied. Where possible, extra information available in VFAINT mode was used to improve the rejection of cosmic ray events. The data were cleaned to remove periods of anomalously high background using the recommended energy ranges and time binning. The net exposure times after cleaning are summarized in Table 1. The analyses of NGC4486 (M87) and NGC6166 have been reported separately by Di Matteo *et al.* (2001, 2003). For these objects, we have used their density and temperature profiles, scaled to the distances summarized in Table 1.

The temperature and density profiles of the X-ray emitting gas were determined using the methods described by Allen *et al.* (2004 and references therein). In brief, concentric annular spectra were extracted from the cleaned event lists, centred on the AGN (identified from radio data and/or the presence of an obvious X-ray point source in the Chandra data). These spectra were analysed using XSPEC (version 11.3: Arnaud 1996), the MEKAL plasma emission code (Kaastra & Mewe 1993; incorporating the Fe-L calculations of Liedhal, Osterheld & Goldstein 1995) and the photoelectric absorption models of Balucinska-Church & McCammon (1992). We have included standard correction factors to account for time-dependent contamination along the instrument light path and have incorporated a small correction to the High Resolution Mirror Assembly model in CIAO 3.2.1, which takes the form of an 'inverse' edge with an energy, E=2.08 keV and optical depth $\tau = -0.1$ (Herman Marshall, private communication). Only data in the $0.6 - 8.0$ keV energy range were used for our analysis. The spectra for all annuli for a particular galaxy were modelled simultaneously in order to determine the deprojected X-ray gas temperature

Table 2. Summary of the Bondi accretion results: the measured velocity dispersions σ, accretion radii $r_{\rm A}$, slopes of the inner electron density profiles α, electron densities at the accretion radii $n_{\rm e}(r = r_{\rm A})$, temperatures at the accretion radii $kT(r = r_{\rm A})$, accretion rates $\dot{M}_{\rm Bondi}$ and predicted accretion powers $P_{\rm Bondi}$.

	$\log\sigma$ (km s^{-1})	$r_{\rm A}$ (pc)	α	$n_{\rm e}(r=r_{\rm A})$ (cm^{-3})	$kT(r=r_{\rm A})$ (keV)	$\dot{M}_{\rm Bondi}$ (10^{-3} M$_\odot$ yr^{-1})	$P_{\rm Bondi}$ (10^{43}erg s^{-1})
NGC507	2.498 ± 0.014	$36.6^{+28.8}_{-16.4}$	$-1.10^{+0.04}_{-0.04}$	$3.43^{+2.89}_{-1.70}$	0.74 ± 0.04	$44.6^{+32.3}_{-19.2}$	$25.3^{+18.3}_{-10.9}$
NGC4374 (M84)	2.473 ± 0.010	$30.2^{+23.1}_{-13.4}$	$-0.55^{+0.19}_{-0.18}$	$0.92^{+0.99}_{-0.47}$	0.71 ± 0.05	$8.47^{+15.63}_{-5.70}$	$4.81^{+8.86}_{-3.23}$
NGC4472	2.488 ± 0.013	$36.0^{+31.9}_{-16.6}$	$-0.36^{+0.12}_{-0.12}$	$0.82^{+0.52}_{-0.29}$	0.70 ± 0.16	$10.8^{+19.2}_{-7.4}$	$6.13^{+10.87}_{-4.17}$
NGC4486 (M87)	2.557 ± 0.013	117^{+122}_{-57}	$-0.00^{+0.10}_{-0.10}$	$0.166^{+0.036}_{-0.032}$	0.80 ± 0.01	$23.7^{+78.7}_{-18.2}$	$13.5^{+44.6}_{-10.3}$
NGC4552 (M89)	2.42 ± 0.13	$17.5^{+46.8}_{-13.3}$	$-0.83^{+0.08}_{-0.08}$	$1.26^{+3.48}_{-0.81}$	0.67 ± 0.09	$4.35^{+14.32}_{-3.68}$	$2.47^{+8.12}_{-2.09}$
NGC4636	2.318 ± 0.017	$9.49^{+8.04}_{-4.25}$	$-0.31^{+0.09}_{-0.09}$	$0.42^{+0.26}_{-0.15}$	0.54 ± 0.11	$4.67^{+13.61}_{-3.71}$	$0.191^{+0.359}_{-0.130}$
NGC4696	2.418 ± 0.014	$15.9^{+12.4}_{-7.0}$	$-0.63^{+0.30}_{-0.30}$	$1.58^{+4.27}_{-1.13}$	0.81 ± 0.05	$0.336^{+0.633}_{-0.230}$	$2.65^{+7.72}_{-2.10}$
NGC5846	2.416 ± 0.012	$19.1^{+14.7}_{-8.5}$	$-0.35^{+0.26}_{-0.21}$	$0.33^{+0.56}_{-0.20}$	0.67 ± 0.09	$1.26^{+3.35}_{-0.94}$	$0.713^{+1.902}_{-0.536}$
NGC6166	2.496 ± 0.012	$20.4^{+30.7}_{-10.4}$	$-0.50^{+0.07}_{-0.06}$	$0.96^{+0.38}_{-0.29}$	1.3 ± 0.7	$5.49^{+11.01}_{-3.63}$	$3.11^{+6.28}_{-2.07}$

profiles, under the assumption of spherical symmetry. [1]. The emission from each spherical shell was modelled as a single phase plasma, with the abundances of all metals assumed to vary with a common ratio, Z, with respect to Solar values in each shell. (The exception to this last assumption was the analysis of NGC4486, reported separately by Di Matteo *et al.* (2003), for which the abundances of key elements were permitted to vary independently in each shell.)

Background spectra were extracted from the blank-field data sets available from the Chandra X-ray Center. These were cleaned in an identical manner to the target observations. In each case, the normalizations of the background files were scaled to match the count rates in the target observations measured in the 9.5-12keV band. Separate photon-weighted response matrices and effective area files were constructed for each region using calibration files appropriate for the period of observation.

Azimuthally-averaged surface brightness profiles were constructed from background subtracted, flat-fielded images with a 0.492×0.492 arcsec^2 pixel scale (1×1 raw detector pixels). Together with the deprojected spectral temperature profiles, these were used to determine the X-ray gas density profiles (see White, Jones & Forman 1997 for details of the technique).

3 CALCULATION OF ACCRETION RATES AND JET POWERS

3.1 Black hole masses and accretion radii

.

For the case of M87, the measurement of the central black hole mass, $M_{\rm BH} = 3.0 \pm 1.0 \times 10^9$ M$_\odot$ is from Tremaine *et al.* (2002) and is based on the data of Harms *et al.* (1994) and Macchetto *et al.* (1997). For the other galaxies in the sample, the black hole masses have been estimated using the correlation between central black hole mass and velocity dispersion, σ, given by Tremaine *et al.* (2002) i.e.

$$\log(M_{\rm BH}/M_\odot) = \alpha + \beta(\log\sigma/200\,{\rm km\,s^{-1}}\ {\rm Mpc^{-1}}), \qquad (1)$$

with $\alpha = 8.13 \pm 0.06$ and $\beta = 4.02 \pm 0.32$. Our analysis uses a Monte Carlo algorithm to account for the uncertainties in the slope of the relation, as well as the intrinsic dispersion of 0.23 dex measured by Tremaine *et al.* (2002). Velocity dispersions for the galaxies are drawn from the work of Bernardi *et al.* (2002) and Mahdavi *et al.* (2001) and are summarized in Table 2.

The accretion radius, $r_{\rm A}$, is the radius within which the gravitational potential of the central black hole dominates over the thermal energy of the surrounding X-ray emitting gas

$$r_{\rm A} = 2GM_{\rm BH}/c_s^2. \qquad (2)$$

Here G is the gravitational constant, $c_s = \sqrt{\gamma_1 kT/\mu m_p}$ is the adiabatic sound speed of the gas at the accretion radius, T is the gas temperature at that radius, $\mu = 0.62$ is the mean atomic weight, m_p is the proton mass and γ_1 is the adiabatic index of the X-ray emitting gas. The results on the accretion radii, summarized in Table 2, account for the uncertainties on the central black hole masses and gas temperatures. The uncertainties in $r_{\rm A}$ are dominated by the uncertainties in $M_{\rm BH}$.

3.2 X-ray gas properties at the accretion radii

Fig 1 shows the electron density profiles for the central regions of the galaxies, determined from the Chandra X-ray data. In cases where the X-ray emission from the innermost parts is contaminated by non-thermal emission from a central AGN (NGC4374, 4486, 4552, 6166), the affected regions have been excluded. The arrows in the figures mark the locations of the accretion radii. With the exception of NGC 4472, the accretion radii are unresolved by the Chandra data. However, in general, the inner few points of the density profiles can be described by a power-law model of the form $n_e(r) \propto r^\alpha$ with $-1.1 < \alpha < 0$ (Table 2). We have used the power-law models to estimate the gas densities at the accretion radii, in each case accounting for uncertainties

[1] Note that for NGC4696, we have only analysed data from a 35 degree wide slice, covering position angles 15-150 degrees. This excludes the complex structure to the west of the central source discussed by Taylor *et al.* 2006). For all other sources, the full 360 degrees of position angle were used. Note that for NGC4686, the bright non-thermal emission from the jets was also excluded (Di Matteo *et al.* 2003)

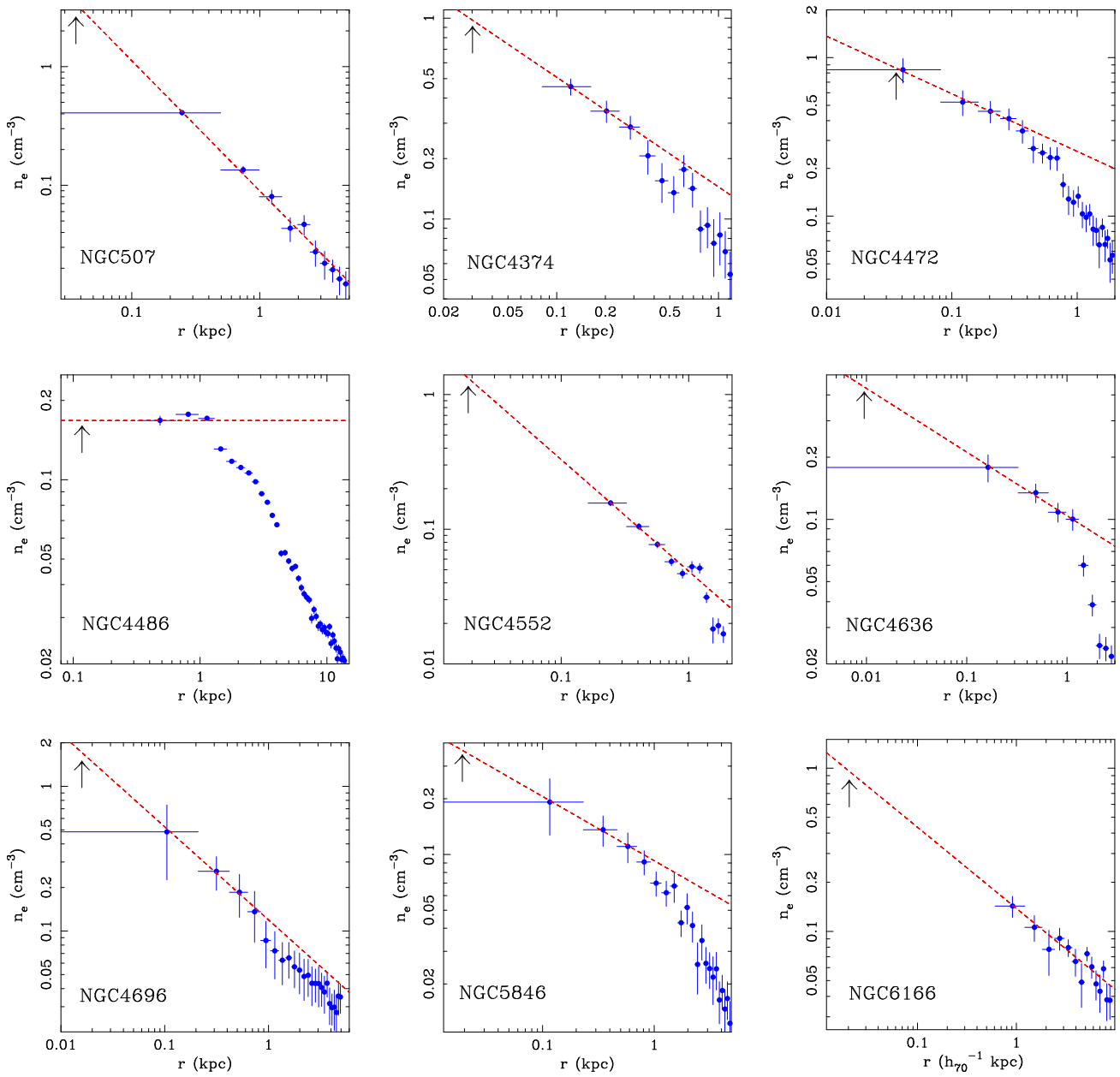

Figure 1. The observed electron density profiles for the central regions of the galaxies, as determined from the Chandra data. For NGC 4374, 4486, 4552 and 6166 the data from the innermost radii, which are contaminated by non-thermal emission from the central AGN, have been excluded. The dashed lines show the best-fitting power law models ($n_e(r) = n_1 r^{\alpha}$) which have been fitted to the inner few bins; the number of bins fitted are noted in parentheses, after the galaxies names below. The Bondi accretion radius, $r_{\rm A}$, for each galaxy is marked with an arrow. From top to bottom, left to right, we show NGC507(10), 4374(3), 4472(4), 4486(1), 4552(3), 4636(4), 4696(4), 5846(3) and 6166(14).

in the slopes and normalizations. For M87 (NGC4486), the density profile flattens within $r \sim 10 r_{\rm A}$ and so we have assumed that the density at $r_{\rm A}$ is equal to the value at the innermost measurement radius. (We assign a systematic uncertainty in the slope $\alpha = 0.0 \pm 0.1$ in this case.) Note that the regions fitted with the power law density models are the regions for which we expect the assumption of spherical symmetry to be most valid, based on the Chandra images,

The temperature profiles for the inner regions of the galaxies are shown in Fig. 2. In general, the profiles do not exhibit steep gradients within $r \sim 10{-}100 r_{\rm A}$. We have therefore assumed that the temperatures at the accretion radii can be estimated from the values at the innermost measurement radii. The temperature results are summarized in Table 2. Systematic uncertainties in the temperature estimates are unlikely to affect other results reported here significantly.

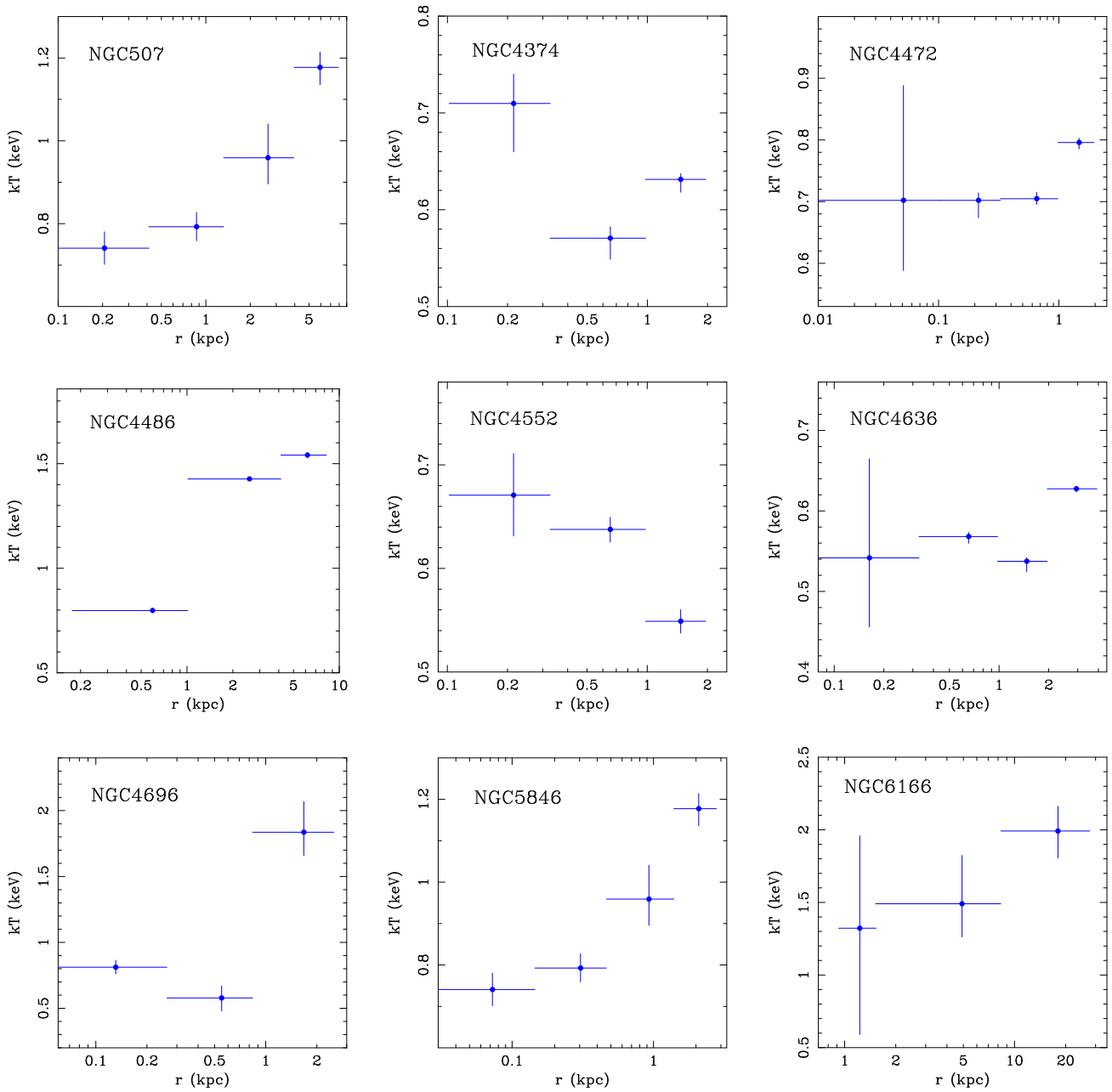

Figure 2. The X-ray gas temperature profiles for the central regions of the galaxies determined from the Chandra data.

3.3 Calculation of the accretion rates

The calculation of accretion rates onto the central black holes follows the work of Bondi (1952). Similar calculations are described by *e.g.* Di Matteo *et al.* (2001, 2003), Churazov *et al.* (2002) and Taylor *et al.* (2005).

Under the assumption of spherical symmetry and negligible angular momentum, the rate of accretion of the X-ray emitting gas at the accretion radii can be written as (Bondi 1952)

$$\dot{M}_{\rm Bondi} = 4\pi\lambda(GM_{\rm BH})^2 c_s^{-3}\rho = \pi\lambda c_s \rho r_{\rm A}^2, \quad (3)$$

where ρ is the density of the gas at the accretion radius (we assume $\rho = 1.13 n_e m_p$) and λ is a numerical coefficient that depends upon the adiabatic index of the accreting gas. For an assumed adiabatic index $\gamma_1 = 5/3$, $\lambda = 0.25$ (Bondi 1952). Note that for $\gamma_1 = 5/3$, $\rho/c_{\rm s}^3$ is constant within the accretion flow, making it appropriate to use the gas temperature and density measured at the accretion radius in our calculations, in place of the values at infinity. (In essence, we are modelling the accretion flows as Bondi flows inward of the accretion radii. For $r > r_{\rm A}$, the gravitational potentials of the galaxies start to dominate and the Bondi formulae become inappropriate.)

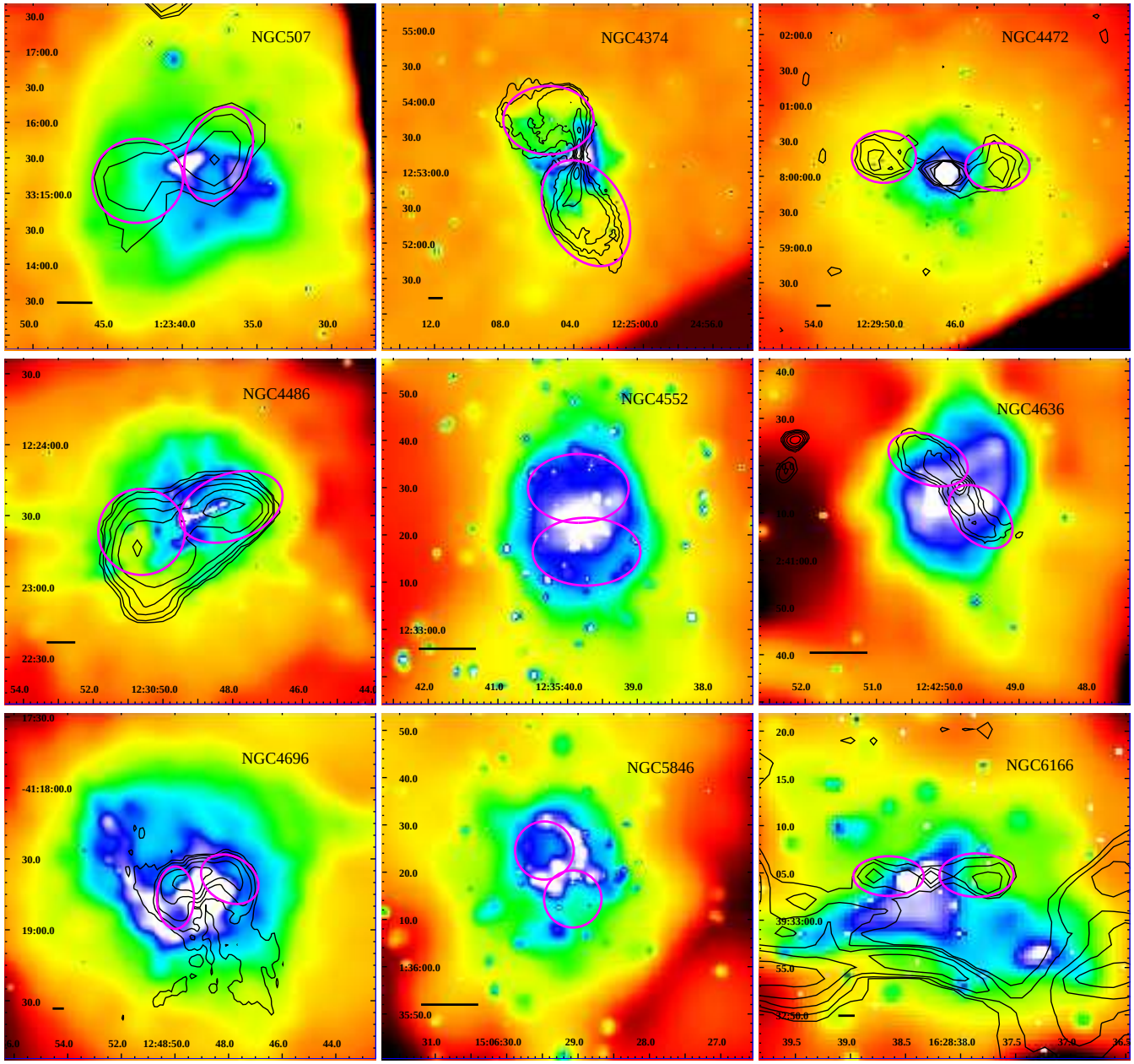

Figure 3. Chandra X-ray images for the central regions of the galaxies. The X-ray images are constructed in the 0.5-8 keV band and have been adaptively smoothed using 2 or 3-pixel Gaussian kernels. The regions identified with the X-ray cavities, which are used to estimate the jet powers, are indicated by bold magenta contours. The narrow black contours show the 1.5 GHz radio emission from archival Very Large Array (VLA) data. The radio data help to identify the cavities in cases where identifications from the X-ray data alone may be ambiguous. The radio contours are logarithmically spaced and have been adjusted to highlight the extended lobe emission. The horizontal scale bar in the bottom left corner of each image denotes a length of 1kpc, except for NGC507 where the scale is 10kpc.

For an efficiency η, relating the accretion rate at the accretion radius to the total energy emitted from within that radius, the maximum power released from the black hole system is

$$P_{\rm Bondi} = \eta \dot{M}_{\rm Bondi} c^2. \quad (4)$$

The values of $P_{\rm Bondi}$, for an assumed value of $\eta = 0.1$ are summarized in Table 2. The uncertainties in the results have been estimated from Monte Carlo simulations, which account for the uncertainties in the σ measurements, the slope and scatter in the $M_{\rm BH} - \sigma$ relation and uncertainties in the temperature and density measurements at the accretion radii. The error budget for $P_{\rm Bondi}$ is dominated by the uncertainties in the $M_{\rm BH}$ estimates.

Table 3. Summary of the jet powers: the distances R from the black holes to the centres of the X-ray bubbles, the energy E required to expand the bubbles, the bubble ages $t_{\rm age}$, and the power required to inflate the bubbles over this timescale $P_{\rm jet}$. The quoted uncertainties in R include statistical measurement errors only. A factor 2 systematic uncertainty in the bubble volumes has been included in the calculation of E and $P_{\rm jet}$.

Galaxy	Lobe	R (kpc)	$E = 4pV$ (10^{54} erg)	$t_{\rm age}$ (10^6 yr)	$P_{\rm jet}$ ($10^{43}\,{\rm erg\,s^{-1}}$)
NGC507	E	12.8 ± 1.0	48900 ± 21100	23.6 ± 2.13	6.60 ± 2.91
	W	11.3 ± 1.0	29300 ± 13300	25.6 ± 2.18	3.62 ± 1.70
NGC4374	N	3.03 ± 0.3	1650 ± 693	6.07 ± 0.56	0.868 ± 0.371
	S	4.36 ± 0.4	2050 ± 854	10.0 ± 1.08	0.658 ± 0.268
NGC4472	E	4.33 ± 0.4	730 ± 287	5.28 ± 0.56	0.445 ± 0.181
	W	3.40 ± 0.3	606 ± 244	5.29 ± 0.57	0.362 ± 0.150
M87	W	1.86 ± 0.05	1210 ± 782	2.92 ± 0.13	1.26 ± 0.84
	E	1.51 ± 0.05	1670 ± 1100	2.38 ± 0.11	2.18 ± 1.44
NGC4552	N	0.58 ± 0.02	35.0 ± 12.7	1.53 ± 0.08	0.0727 ± 0.0274
	S	0.58 ± 0.02	39.4 ± 14.3	1.51 ± 0.08	0.0829 ± 0.0307
NGC4636	NE	0.69 ± 0.07	8.10 ± 3.21	1.77 ± 0.15	0.0147 ± 0.0060
	SW	0.66 ± 0.07	8.04 ± 3.25	1.68 ± 0.17	0.0152 ± 0.0060
NGC4696	E	2.49 ± 0.3	601 ± 338	6.06 ± 0.66	0.313 ± 0.177
	W	3.00 ± 0.3	826 ± 438	5.54 ± 0.60	0.478 ± 0.244
NGC5846	N	0.72 ± 0.12	21.0 ± 11.2	1.81 ± 0.30	0.0367 ± 0.0185
	S	0.72 ± 0.12	20.8 ± 11.3	1.81 ± 0.30	0.0374 ± 0.0188
NGC6166	E	2.30 ± 0.10	829 ± 336	3.51 ± 0.27	0.741 ± 0.316
	W	2.40 ± 0.10	981 ± 383	3.66 ± 0.28	0.838 ± 0.353

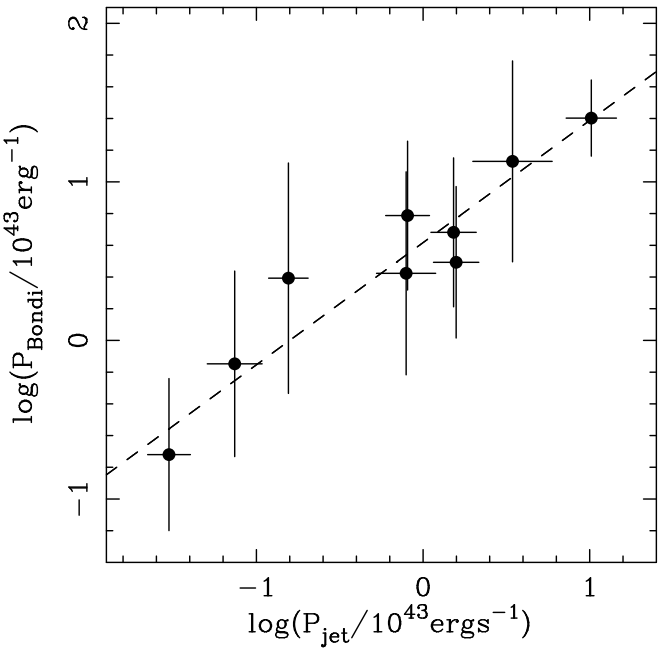

Figure 4. The logarithm of the Bondi accretion power (in units of $10^{43}\,{\rm erg\,s^{-1}}$) determined from the Chandra X-ray data, assuming an efficiency $\eta = 0.1$ for the conversion of rest mass into energy, versus the logarithm of the jet power (also in units of $10^{43}\,{\rm erg\,s^{-1}}$). The dashed line is the best-fitting linear-plus-constant model determined using the χ^2 estimator, as described in the text.

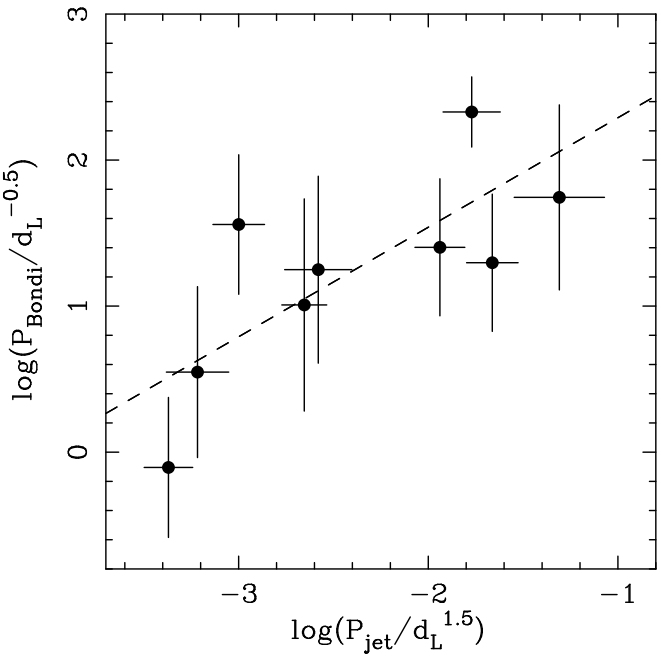

Figure 5. The logarithm of the Bondi accretion power versus the logarithm of the jet power, with the distance dependences removed. Both powers are in units of $10^{43}\,{\rm erg\,s^{-1}}$, with the distances in Mpc. The dashed line is the best-fitting linear-plus-constant model determined using the BCES estimator. A clear correlation between the plotted quantities remains and the reduced χ^2 value indicates that a power law model provides an acceptable description of the data.

3.4 Calculation of jet power

To estimate the kinetic power of the jets, we first estimated the energy, E required to create the observed bubbles in the X-ray emitting gas. For slow expansion rates, this is the sum of the internal energy within the bubble and the $P\mathrm{d}V$ work done

$$E = \frac{1}{\gamma_2 - 1} PV + PV = \frac{\gamma_2}{\gamma_2 - 1} PV, \quad (5)$$

where P is the thermal pressure of the surrounding, X-ray emitting gas (which can be determined from the observed X-ray temperatures and densities), V is the volume of the cavity and γ_2 is the mean adiabatic index of the fluid within the cavity. For the case of a bubble filled with relativistic plasma, $\gamma_2 = 4/3$ and $E = 4PV$. Some additional energy will also be transfered into sound waves (Churazov *et al.* 2002; Fabian *et al.* 2003, 2005a,b; Forman *et al.* 2003; Ruszkowski *et al.* 2004). We have neglected this extra energy in our calculations, although the power involved is likely to be smaller than the quoted uncertainties on the jet powers.

The regions identified with the bubbles are shown in Fig. 3. In general, the bubbles appear to be 'attached' to the central AGN and are likely to be undergoing expansion at present. A possible exception to this is NGC4472, where the bubbles may have recently detached. In cases where the edges of the bubbles are not clearly defined in the X-ray data, we have used radio observations to estimate their volumes (Fig. 3). The X-ray and radio data show that in general, the bubbles or cavities are approximately elliptical. We have therefore parameterized the projected areas of the bubbles in terms of a semi-axis length, r_l, along the jet direction and semi-axis width, r_w, across it. This allows the cavities to be modelled as ellipsoids with volumes $V = 4\pi r_\mathrm{l} r_\mathrm{w} r_\mathrm{d}/3$, where r_d is the unknown depth of the cavity along the line of sight. We model the cavities as prolate ellipsoids with $V = 4\pi r_\mathrm{l} r_\mathrm{w}^2/3$, although systematic uncertainties in r_l, r_w and, especially, r_d mean that our estimates of the bubble volumes should be regarded as uncertain at the factor ~ 2 level.

Following Birzan *et al.* (2004; see also Dunn & Fabian 2004, Dunn, Fabian & Taylor 2005) we have estimated the ages of the bubbles as

$$t_\mathrm{age} = R/c_s, \quad (6)$$

where R is the distance of the bubble centre from the black hole, which provides a reasonable match to some numerical simulations. We note that the bubbles have lower mass density than the surrounding X-ray emitting gas and can therefore be expected to rise with a buoyancy velocity, $v_\mathrm{b} = \sqrt{2gV/SC_D}$. Here $S = \pi r_\mathrm{w}^2$ is the cross-sectional area of the bubble (in the rise direction), V is the volume, $C_D \sim 0.75$ is the drag coefficient and $g = GM(<R))/R^2$ is the gravitational acceleration. The times required for bubbles of the observed sizes to rise buoyantly through a uniform medium from the galaxy centres to their current radii is approximately $t_\mathrm{buoy} = R/v_\mathrm{b}$. Application of this formula leads to comparable timescales to the t_age values. However, since the bubbles studied here are typically still attached to the jets, we adopt t_age as our relevant timescale.

The power involved in 'blowing' the bubbles can be estimated as

$$P_\mathrm{jet} = E/t_\mathrm{age}. \quad (7)$$

The results on P_jet are summarized in Table 2. The uncertainties on P_jet are determined from Monte Carlo simulations which include the sources of statistical uncertainty mentioned above as well as a factor 2 systematic uncertainty in the bubble volumes.

4 THE RELATION BETWEEN ACCRETION RATE AND JET POWER

Fig 4 shows the results on the accretion power P_Bondi, for an assumed efficiency $\eta = 0.1$ for the conversion of accreted rest mass into energy, versus the jet power, P_jet, determined from the bubble properties. Both powers are in units of $10^{43}\,\mathrm{erg\,s^{-1}}$. For each galaxy, we have combined the power estimates for both bubbles, with the uncertainties added in quadrature. A clear correlation between the P_Bondi and P_jet exists, which can be described by a power law model of the form

$$\log \frac{P_\mathrm{Bondi}}{(10^{43}\,\mathrm{erg\,s^{-1}})} = A + B \log \frac{P_\mathrm{jet}}{(10^{43}\,\mathrm{erg\,s^{-1}})}. \quad (8)$$

Using the χ^2 fit statistic, which accounts only for errors in the P_Bondi values (which are larger, typically, than the uncertainties in P_jet), we find $A = 0.62 \pm 0.15$ and $B = 0.77 \pm 0.18$, with $\chi^2 = 1.2$ for 7 degrees of freedom. (The quoted uncertainties on α and β are 68 per cent confidence intervals.) Using the BCES($Y|X$) estimator of Akritas & Bershady (1996), which accounts for errors in both axes and the presence of possible intrinsic scatter, we obtain $A = 0.64 \pm 0.08$ and $B = 0.77 \pm 0.17$. The average deviation about the best fitting model is $\sigma(\log P_\mathrm{Bondi}) = 0.16$.

The results in Fig 4 indicate the presence of a strong correlation between P_Bondi and P_jet. The power-law model provides a good description of the data; indeed the χ^2 value obtained is unusually low. However, we must also consider that the plotted quantities have some variables in common. Most importantly, both P_Bondi and P_jet depend on the distances to the objects, with $P_\mathrm{Bondi} \propto d_\mathrm{L}^{-0.5}$ and $P_\mathrm{jet} \propto d_\mathrm{L}^{1.5}$. This distance dependence should introduce a mild anticorrelation between the results. Fig 5 shows a plot of $P_\mathrm{Bondi}/d_\mathrm{L}^{-0.5}$ versus $P_\mathrm{jet}/d_\mathrm{L}^{1.5}$. In this case the dispersion is increased to an acceptable value, $\chi^2 = 10.6$ for 7 degrees of freedom, and a clear, almost linear, correlation remains with $B = 0.91 \pm 0.23$. (Using the BCES estimator in place of χ^2, we measure $B = 0.75 \pm 0.27$.)

Both axes in Fig 4 also depend on the temperature T of the X-ray emitting gas. However, the temperature shows little variation from object to object and varies only mildly with radius between the accretion and bubble radii. Moreover, the dependences on temperature are approximately $P_\mathrm{Bondi} \propto T^{-1.5}$ and $P_\mathrm{jet} \propto T^{1.5}$, which should also introduce a mild anti-correlation. Finally, both axes involve the gas density, measured at the accretion radius for P_Bondi and at the bubble centres for P_jet. These radii are very different and the density profiles vary significantly from object to object, meaning that the densities are essentially uncorrelated. (In detail, a mild anticorrelation is observed).

We conclude that the observed correlation between P_Bondi and P_jet indicates a tight physical connection between the two quantities.

5 IMPLICATIONS AND DISCUSSION

We have shown that for supermassive black holes at the centres of large, X-ray luminous elliptical galaxies, a remarkable, tight correlation exists between the 'Bondi' accretion rates inferred from the Chandra X-ray data and observed galaxy velocity dispersions, and the power emerging from these systems in relativistic jets. Our result has important implications for the nature of the accretion process and for issues relating to feedback, the growth of black holes and galaxy formation.

The relationship between the Bondi accretion power and jet power can be described by a power law model of the form $\log P_{\rm Bondi} = 0.62(\pm0.15) + 0.77(\pm0.18)\log P_{\rm jet}$, where $P_{\rm Bondi} = 0.1\dot{M}_{\rm Bondi}c^2$ and $P_{\rm jet}$ is the power associated with inflating the cavities and providing the internal energy of the plasma that fills them. A significant fraction ($2.4^{+1.0}_{-0.7}$ per cent, for $P_{\rm jet} = 10^{43}\,{\rm erg\,s^{-1}}$) of the energy associated with the rest mass of material entering the Bondi accretion radius emerges from the systems in relativistic jets. There is a mild evidence that this fraction increases as $P_{\rm jet}$ rises, from $1.4^{+0.9}_{-0.5}$ per cent at $P_{\rm jet} = 10^{42}\,{\rm erg\,s^{-1}}$, to $4.1^{+1.6}_{-1.2}$ per cent at $P_{\rm jet} = 10^{44}\,{\rm erg\,s^{-1}}$.

The existence of such a tight correlation suggests that the Bondi formalism provides a reasonable description of the accretion process in these systems, despite the fact that the accreting gas contains magnetic fields (*e.g.* Taylor *et al.* 2005) and, presumably, has some angular momentum. Moreover, the similarity of the $P_{\rm jet}$ and $P_{\rm Bondi}$ values suggests that a significant fraction of the matter passing through the accretion radius flows all the way down to regions close to the black hole, where it presumably provides the power source for the jets. This provides an important constraint on both accretion and jet formation models. In particular, our results limit the amount of material that may be lost from the accretion flows en route to the region of jet formation and requires that jet formation must be efficient; a few per cent of the energy associated with the rest mass of material entering the accretion radius emerges in the jets.

The origin of the jets may be related to the spin of the central black hole (*e.g.* Rees 1978; Hughes & Blandford 2003). In that case, the observed tight correlation between jet power and accretion rate may suggest a narrow range of black hole spins for the objects in our sample. The X-ray emitting gaseous halos in the giant elliptical galaxies studied here are likely to have existed for billions of years. The growth of the black holes may therefore have been dominated by gas accretion, which tends to lead to large spin parameters (*e.g.* Volonteri *et al.* 2005) and it is therefore possible that the black holes are rotating at close to their maximal rates. However, the detailed interaction between accretion, spin-up and jet power remains to be explored.

The tight correlation between $P_{\rm Bondi}$ and $P_{\rm jet}$ also suggests that the accretion flows in the galaxies are stable over the periods required for gas to flow from the accretion radii to the base of the jets *plus* the times required for the bubbles to be inflated. The flow times $t_{\rm flow} \sim r_{\rm A}/c_s$ are of the order a few 10^4 to a few 10^5 yr, whereas the bubble ages range from $10^6 - 2\times10^7$ yr (Table 3). Thus, our results suggest that the accretion flows in the present sample of objects are approximately stable over timescales of $10^6 - 10^7$ yr.

The black holes studied here are accreting at rates of a few 10^{-4} to a few $10^{-2}\,{\rm M_\odot\,yr^{-1}}$ and converting a few per cent of their accreted rest mass into jet energy. The nuclear luminosities (Pellegrini 2005) are typically 2-4 orders of magnitude lower than the $P_{\rm jet}$ values, so the systems are 'quiescent' in terms of their nuclear luminosities. (Orientation and obscuration effects will play some role although are unlikely to modify this conclusion *e.g.* Di Matteo *et al.* 2001, 2003; Allen, Di Matteo & Fabian 2000.) It is interesting to note that the measured jet powers are comparable to the bolometric luminosities predicted by standard, radiatively efficient accretion disk models with $\eta \sim 0.1$ (Shakura & Sunyaev 1973). Thus, it is possible that the ratio of accretion rate/total emitted power (bolometric luminosity plus jet power) may remain relatively stable as the accretion mode varies from a quasar to optically quiescent phase.

Our results have significant implications for models of galaxy formation and support the idea that feedback from central black holes is important in shaping the bright end of the galaxy luminosity function (see Croton *et al.* 2005 and Bower *et al.* 2005 for recent discussions). The *observed* efficiency with which energy associated with the rest mass of accreted matter is fed back into the surrounding X-ray emitting gas via the jets is similar to that *assumed* in the semi-analytic models of *e.g.* Croton *et al.* (2005). These models have been shown to be able to explain the exponential cut off at the bright end of the galaxy luminosity function and the fact that the most massive galaxies tend to be bulge dominated systems in clusters, containing systematically older stars.

Our results show that the supermassive black holes in elliptical galaxies are prodigious energy sources, with the bulk of the energy emerging in the form of relativistic jets rather than radiation. In order for this energy to be coupled back into the surrounding matter, the jets must have a working surface which is provided in these cases by the X-ray emitting gas. For the elliptical galaxies studied here, the power fed back into the X-ray emitting gas is sufficient to offset cooling and heat the gas, thereby preventing further star formation. Since we expect all large galaxies to contain a supermassive black hole, even at high redshifts, this suggests that a key stage in the formation of such galaxies will be when they first become large enough to maintain an X-ray gaseous halo. (This then provides a working surface for the jets, allowing feedback and preventing further galaxy growth. Although the jets will have been providing power before this point, they are unlikely to have had an effective working surface.) Note, however, that although star formation is truncated when jet feedback becomes efficient, the black hole may continue to grow via accretion from the X-ray gas at approximately the Bondi rate.

A closely related topic is that of cooling flows in galaxies and clusters, and the mechanism responsible for preventing gas cooling to low temperatures ($kT \lesssim 1$keV). As stated above, the $P_{\rm jet}$ values in the galaxies and groups studied here are sufficient to offset further cooling of the X-ray gas. It is interesting to consider extending the correlation between $P_{\rm Bondi}$ and $P_{\rm jet}$ to larger systems where the cooling of the gas is more rapid. For the largest cooling flow clusters, the cooling luminosity exceeds $10^{45}\,{\rm erg\,s^{-1}}$. If the black hole masses and accretion rates in these galaxies are not significantly larger than in NGC507 and M87, then the jet power is unlikely to be sufficient to balance cooling and some cooling

to very low temperatures and associated star formation can be expected to occur (see also Fabian *et al.* 2002). This is consistent with observations indicating the presence of vigorous star formation and large molecular gas concentrations in the largest cooling flow clusters, but not in smaller, less X-ray luminous systems (Allen 1995; Crawford *et al.* 1999; Edge 2001).

Finally, we note that although systematic uncertainties have been included in the extrapolation of the gas properties to the Bondi radii and in our calculation of the bubble volumes, other sources of systematic uncertainty remain. For example, the assumption that $\lambda = 0.25$ in the calculation of $P_{\rm Bondi}$ may not be precise, and our assumption that the bubble ages can be estimated as $t_{\rm age}$ is probably uncertain at the factor ~ 2 level. However, we do not expect such uncertainties to affect the main conclusions drawn here.

ACKNOWLEDGEMENTS

We thank Roger Blandford, Glenn Morris and Bob Wagoner for helpful discussions. This work was supported in part by the U.S. Department of Energy under contract number DE-AC02-76SF00515. RD and ACF thank PPARC and the Royal Society for support, respectively. GBT acknowledges support from the National Aeronautics and Space Administration through Chandra Award Number GO4-5135X issued by the Chandra X-ray Observatory Center, which is operated by the Smithsonian Astrophysical Observatory for and on behalf of the National Aeronautics and Space Administration under contract NAS8-03060. The National Radio Astronomy Observatory is a facility of the National Science Foundation operated under a cooperative agreement by Associated Universities, Inc.

REFERENCES

Allen S.W., 1995, MNRAS, 276, 947
Allen S.W., Di Matteo T., Fabian A.C., 2000, MNRAS, 311, 493
Allen S.W., Ettori S., Fabian A.C., 2001, MNRAS, 324, 877
Allen S.W., Schmidt R.W., Ebeling H., Fabian A.C., van Speybroeck L., 2004, MNRAS, 353, 457
Akritas M.G., Bershady M.A., 1996, ApJ, 470, 706
Arnaud, K.A., 1996, in Astronomical Data Analysis Software and Systems V, eds. Jacoby G. and Barnes J., ASP Conf. Series volume 101, p17
Balucinska-Church M., McCammon D., 1992, ApJ, 400, 699
Benson A.J., Bower R.J., Frenk C.S., Lacey C.G., Baugh C.M., Cole S., 2003, ApJ, 599, 38
Bernardi M., Alonso M.V., da Costa L.N., Willmer C.N.A., Wegner G., Pellegrini P.S., Rite C., Maia M.A.G., 2002, AJ, 123, 2990
Birzan L., Rafferty D.A., McNamara B.R., Wise M.W., Nulsen P.E.J., 2004, ApJ, 607, 800
Böhringer H., Voges W., Fabian A.C., Edge A.C., Neuman D.M., 1993, MNRAS, 264, 25
Bondi H., 1952, 112, 195
Bower R.G., Benson A.J., Malbon R., Helly R., Frenk C.S., Baugh C.M., Cole S., Lacey C.G., 2005, MNRAS, submitted (astro-ph/-511338)
Churazov E., Brüggen M., Kaiser C.R., Böhringer H., Forman W., 2001, ApJ, 554, 261
Churazov E., Sunyaev R., Forman W., Böhringer H., 2002, MNRAS, 332, 729
Crawford C.S., Allen S.W. Ebeling H., Edge A.C., Fabian A.C., 1999, MNRAS, 306, 857
Croton *et al.* 2005, MNRAS, in press (astro-ph/0508046)
Di Matteo T., Allen S.W., Fabian A.C., Wilson A.S., Young A.J., 2003, ApJ, 582, 133
Di Matteo T., Johnstone R.M., Allen S.W., Fabian A.C., 2001, ApJ, 550, L19
Dunn R.J.H., Fabian A.C., 2004, MNRAS, 355, 862
Dunn R.J.H., Fabian A.C., Taylor G.B., 2005, MNRAS, in press (astro-ph/0510191)
Edge A.C., 2001. MNRAS, 328, 762
Fabian A.C., Reynolds C.S., Taylor G.B., Dunn R.J.H., 2005a, MNRAS, 363, 891
Fabian A.C., Sanders J.S., Taylor G.B., Allen S.W., Crawford C.S., Johnstone R.M., Iwasawa K., 2005b, MNRAS, submitted (astro-ph/0510476)
Fabian A.C., Sanders J.S., Allen S.W., Crawford C.S., Iwasawa K., Johnstone R.M., Schmidt R.W., Taylor G.B., Dunn R.J.H., 2003, MNRAS, 344, L43 Schmidt R.W., Taylor G.B., Dunn R.J.H., 2003, MNRAS, 344, L43
Fabian A.C., Allen S.W., Crawford C.S., Johnstone R.M., R.J. Morris, J.S. Sanders, Schmidt R.W., 2002, MNRAS, 332, L50
Fabian A.C., Sanders J.S., Ettori S., Taylor G.B., Allen S.W., Crawford C.S., Iwasawa K., Johnstone R.M., Ogle P.M., 2000, MNRAS,, 318, L65
Forman W. *et al.* , 2006, ApJ, submitted (astro-ph/0312576)
Harms R.J. *et al.* 1994, ApJ, 435, L35
Hughes S.A., Blandford R.D., 2003, ApJ, 585, L101
Kaastra J.S., Mewe R., 1993, Legacy, 3, HEASARC, NASA
Liedhal D.A., Osterheld A.L., Goldstein W.H., 1995, ApJ, 438, L115
Macchetto F., Marconi A., Axon D.J., Capetti A., Sparks W., Crane P., 1997, ApJ, 489, 579
Mahdavi A., Geller M.G., 554, L129
Pellegrini S., 2005, ApJ, 624, 155
Peterson J.R. *et al.* 2001, A&A, 365, L104
Peterson J.R., Kahn S.M., Paerels F.B.S., Kaastra J.S., Tamura T., Bleeker J.A.M., Ferrigno C., Jernigaan J.G., 2003, ApJ, 590, 207
Rees M.J., 1978, Nature, 275, 516
Ruszkowski M., Brüggen M., Begelman M.C., 2004, ApJ, 611, 158
Shakura N.I., Sunyaev R.A., 1973, A&A, 24, 337
Tamura T. *et al.* 2001, A&A, 365, L87
Taylor G.B., Sanders J.S., Fabian A.C., Allen S.W., 2006, MNRAS, 365, 705
Tremaine S. *et al.* 2002, ApJ, 574, 740
Volonteri M., Madau P., Quataert E., Rees M.J., 2005, ApJ, 620, 69
White D.A., Jones C., Forman W., 1997, MNRAS, 292, 419